

## PROPOSAL

**Determination of the neutron fluence, the beam characteristics  
and the backgrounds at the CERN-PS TOF Facility**

*The n-TOF Collaboration*

R.L. Aguiar<sup>26)</sup>, S. Andriamonje<sup>5)</sup>, A. Angelopoulos<sup>15)</sup>, P. Assimakopoulos<sup>16)</sup>, L. Audouin<sup>7)</sup>, G. Badurek<sup>2)</sup>, G. Bakos<sup>18)</sup>, P. Baumann<sup>10)</sup>, H. Beer<sup>12)</sup>, J. Benlliure Anya<sup>33)</sup>, J.M. Benlloch<sup>35)</sup>, S. Boffi<sup>23)</sup>, A. Boiano<sup>22)</sup>, C. Borcea<sup>37)</sup>, A. Brusegan<sup>3)</sup>, F. Calvino<sup>30)</sup>, C.F. Cambronero<sup>33)</sup>, D. Cano-Ott<sup>31)</sup>, P. Cennini<sup>37)</sup>, G. Charpak<sup>8)</sup>, V. Chepel<sup>27)</sup>, N. Colonna<sup>19)</sup>, G. Cortes<sup>30)</sup>, F. Corvi<sup>3)</sup>, J.L. Cura<sup>26)</sup>, S. Czajkowski<sup>5)</sup>, C.H. Dasso<sup>34)</sup>, S. David<sup>7)</sup>, A. De Blas<sup>30)</sup>, M. De Poli<sup>21)</sup>, R. Del Moral<sup>5)</sup>, J.P. Delaroche<sup>4)</sup>, G. Della Mea<sup>21)</sup>, J. Derre<sup>9)</sup>, S. Diez<sup>31)</sup>, R. Dolfini<sup>23)</sup>, I. Duran Escribano<sup>33)</sup>, C. Eleftheriadis<sup>17)</sup>, M. Embid Segura<sup>31)</sup>, F. Farget<sup>7)</sup>, A. Ferrari<sup>37)</sup>, R. Ferreira Marques<sup>27)</sup>, W. Furman<sup>28)</sup>, A. Gadea<sup>35)</sup>, J.A. Garzon<sup>33)</sup>, I. Giomataris<sup>9)</sup>, C. Giusti<sup>23)</sup>, E.M. Gonzalez-Romero<sup>31)</sup>, A. Goverdovski<sup>29)</sup>, F. Gramegna<sup>21)</sup>, E. Griesmayer<sup>1)</sup>, O. Grudzevich<sup>29)</sup>, K.H. Guber<sup>32)</sup>, N. Gundrorin<sup>28)</sup>, F. Gunsing<sup>9)</sup>, M. Hage-Ali<sup>11)</sup>, B. Haight<sup>40)</sup>, S. Harissopoulos<sup>14)</sup>, M. Heil<sup>12)</sup>, K.G. Ioannides<sup>16)</sup>, P.D. Ioannou<sup>15)</sup>, S. Isaev<sup>29)</sup>, J. Jastrebski<sup>25)</sup>, E. Jericha<sup>2)</sup>, Y. Kadi<sup>37)</sup>, F. Kaeppler<sup>12)</sup>, C. Kalfas<sup>14)</sup>, D. Karamanis<sup>5)</sup>, L. Kazakov<sup>29)</sup>, A. Kelic<sup>10)</sup>, V. Ketlerov<sup>29)</sup>, G. Kitis<sup>17)</sup>, P.E.J. Koehler<sup>39)</sup>, V. Konovalov<sup>28)</sup>, I. Kopatch<sup>28)</sup>, E. Kossionides<sup>14)</sup>, V. Lacoste<sup>37)</sup>, L.C. Leal<sup>39)</sup>, H. Leeb<sup>2)</sup>, A. Lepretre<sup>9)</sup>, M.I. Lopes<sup>27)</sup>, M. Lozano<sup>34)</sup>, J.M. Martinez-Val<sup>32)</sup>, P. Mastinu<sup>21)</sup>, M.F. Matteucci<sup>24)</sup>, D. Matveev<sup>28)</sup>, A. Mengoni<sup>20)</sup>, R. Meunier<sup>6)</sup>, P.M. Milazzo<sup>24)</sup>, E. Minguez Torres<sup>32)</sup>, V. Mitrofanov<sup>29)</sup>, A. Molina<sup>34)</sup>, R. Mordenti<sup>22)</sup>, O. Morra<sup>19)</sup>, P. Mutti<sup>3)</sup>, P.J. Napiorkowski<sup>25)</sup>, N. Nicolis<sup>16)</sup>, R. Nolte<sup>13)</sup>, H. Oberhammer<sup>2)</sup>, A. Ordine<sup>22)</sup>, F.D. Pacati<sup>23)</sup>, A.A. Pakou<sup>16)</sup>, T. Papaevangelou<sup>17)</sup>, T. Paradelis<sup>14)</sup>, V. Paticchio<sup>19)</sup>, A. Pavlik<sup>2)</sup>, P. Pavlopoulos<sup>36)</sup>, J.M. Perlado<sup>32)</sup>, M. Piera<sup>32)</sup>, V. Piksakin<sup>29)</sup>, A. Plompen<sup>3)</sup>, A. Poch<sup>30)</sup>, A. Policarpo<sup>27)</sup>, A. Popov<sup>28)</sup>, Y. Popov<sup>28)</sup>, C. Pretel<sup>30)</sup>, A. Quaranta<sup>24)</sup>, J.M. Quesada<sup>34)</sup>, E. Radermacher<sup>37)</sup>, M. Radici<sup>23)</sup>, S. Raman<sup>39)</sup>, G. Rapp<sup>12)</sup>, T. Rauscher<sup>36)</sup>, R. Reifarh<sup>12)</sup>, V. Rigato<sup>21)</sup>, J. Robin<sup>10)</sup>, C. Rubbia<sup>23)</sup>, B. Rubio<sup>35)</sup>, G. Rudolf<sup>10)</sup>, P. Rullhusen<sup>3)</sup>, B. Rundberg<sup>40)</sup>, L. Sakelliou<sup>15)</sup>, F. Saldana<sup>37)</sup>, D.M. Santos<sup>26)</sup>, J. Sanz<sup>32)</sup>, E. Savvidis<sup>17)</sup>, S. Savvidis<sup>18)</sup>, H. Schuhmacher<sup>13)</sup>, P. Sedyshev<sup>28)</sup>, D. Serov<sup>28)</sup>, C. Stephan<sup>7)</sup>, G. Tagliente<sup>19)</sup>, J.L. Tain<sup>35)</sup>, C. Tapia<sup>30)</sup>, L. Tassan-Got<sup>7)</sup>, M. Terrani<sup>23)</sup>, R. Tertychny<sup>29)</sup>, N. Tsagas<sup>18)</sup>, A. Tzima<sup>17)</sup>, A. Valentino<sup>19)</sup>, E. Vardaci<sup>22)</sup>, A. Ventura<sup>20)</sup>, D. Villamarin<sup>31)</sup>, V. Vlachoudis<sup>37)</sup>, A.V. Voinov<sup>28)</sup>, F. Voss<sup>12)</sup>, H. Weigmann<sup>3)</sup>, H. Wendler<sup>37)</sup>, M.C. Wiescher<sup>38)</sup>, K. Wisshak<sup>12)</sup>, S. Zeinalov<sup>28)</sup>

---

<sup>1)</sup> Technische Fachhochschule Neustadt, Wien, Austria

<sup>2)</sup> Institut für Kernphysik, Technische Universität, Wien, Austria

<sup>3)</sup> IRMM, European Commission Joint Research Centre, Geel, Belgium

<sup>4)</sup> CEA, Bruyeres-le-Chatel, France

<sup>5)</sup> CEN, Bordeaux-Gradignan, France

<sup>6)</sup> CSNSM, Orsay, France

<sup>7)</sup> IPN, Orsay, France

- 
- 8) Ecole Supérieure de Physique et Chimie Industrielle (ESPCI), Paris, France
  - 9) DSM/DAPNIA, CEA, Saclay, France
  - 10) IRES, Strasbourg, France
  - 11) CNRS-PHASE, Strasbourg, France
  - 12) Institut für Kernphysik, FZK Karlsruhe, Germany
  - 13) Physikalisch-Technische Bundesanstalt (PTB), Braunschweig, Germany
  - 14) NCSR “Demokritos”, Institute of Nuclear Physics, Athens, Greece
  - 15) University of Athens, Division of Nuclear Physics, Greece
  - 16) University of Ioannina, Nuclear Physics Laboratory, Greece
  - 17) Aristotle University, Department of Physics, Thessaloniki, Greece
  - 18) Democritian University of Thrace, Xanthi, Greece
  - 19) Università di Bari e Sezione dell’INFN, Italy
  - 20) ENEA, Bologna, Italy
  - 21) INFN, Laboratori Nazionali di Legnaro, Italy
  - 22) Università di Napoli e Sezione dell’INFN, Italy
  - 23) Università di Pavia e Sezione dell’INFN, Italy
  - 24) Università di Trieste e Sezione dell’INFN, Italy
  - 25) Heavy Ion Lab., University of Warsaw, Poland
  - 26) Universidade de Aveiro, Aveiro, Portugal
  - 27) Universidade de Coimbra, Coimbra, Portugal
  - 28) Joint Institute for Nuclear Research, Frank Laboratory of Neutron Physics, Dubna, Russia
  - 29) Institute of Physics and Power Engin., Division of Nuclear and Neutron Physics, Obninsk, Russia
  - 30) SCN-FEN, Universidad Politécnica de Catalunya, Barcelona, Spain
  - 31) CIEMAT, Madrid, Spain
  - 32) Instituto de Fusión Nuclear, Universidad Politécnica de Madrid, Spain
  - 33) Universidad de Santiago de Compostela, Spain
  - 34) Universidad de Sevilla, Spain
  - 35) Instituto de Física Corpuscular, Universidad de Valencia, Spain
  - 36) University of Basel, Switzerland
  - 37) CERN, Geneva, Switzerland
  - 38) University of Notre Dame, USA
  - 39) Oak Ridge National Laboratory, USA
  - 40) Los Alamos National Laboratory, USA

## 1 Introduction

In the scope of our programme [1] we propose to start in July 2000 with measurements on elements of well known cross sections, in order to check the reliability of the whole experimental installation at the CERN-TOF facility. These initial exploratory measurements will provide the key-parameters required for the further experimentation at the CERN-TOF neutron beam. The neutron fluence and energy resolution will be determined as a function of the neutron kinetic energy by reproducing standard capture and fission cross sections. The measurements of capture cross section on elements with specific cross section features will allow to us to disentangle the different components of backgrounds and estimate their level in the experimental area. The time-energy calibration will be determined and monitored with a set of monoenergetic filters as well as by the measurements of elements with resonance-dominated cross sections. Finally, in this initial phase the behaviour of several detectors scheduled in successive measurements should be in situ tested.

## 2 The neutron fluence and its energy dependence

In neutron time-of-flight spectroscopy the detector needs to register only the arrival time of a neutron and the information on the energy realised by neutron interaction would only serve to determine and reduce the possible backgrounds.

The quantity determined in a neutron cross section experiment is the reaction yield, i.e. the fraction of neutrons incident on a sample and undergoing the interaction under study. We intend to use several techniques to measure neutron fluences over the desired energy range from 1 eV to over 250 MeV. These techniques making use of the neutron induced reaction cross sections considered as "standards", will allow us to obtain a coherent and redundant set of neutron fluence measurements. Such neutron flux detectors will serve for the experimental determination of the neutron fluence, in particular in relation with the proton beam intensity, and will permanently monitor the intensity of the neutron beam. In fact, for determining the neutron induced reaction cross section of the sample under study, only the knowledge of the shape of the neutron flux as a function of the time-of-flight is required but not its absolute value. Because the energy dependent scaling factor for the determination of the absolute fluence is conveniently taken by the fitted normalisation of the measurements on elements with well known (standard) reaction cross sections. Such measurements of "standards" will be either simultaneous or alternatively performed on-line with the measurement of the sample under study. In this way we will obtain the determination of the incident neutron fluence, i.e. the flux integrated over the measurement time, required for the reconstruction of the reaction yield from the measured time-of-flight spectra.

Flux measurements are based on reactions with smooth standard cross sections, notably  $^{10}\text{B}(n,\alpha)^7\text{Li}$  and  $^6\text{Li}(n,\alpha)^3\text{H}$  considered as a standard from thermal up to 250 keV and 1 MeV respectively, as well as  $^{235}\text{U}(n,f)$  being "standard" from 0.15 to 20 MeV [2]. These reactions can be measured with a different detector at the same time as the samples under investigation. This way of flux measurement is a common practise in measurements of neutron induced reaction cross sections. In the unresolved region, it is possible to measure the flux by the  $^{197}\text{Au}(n,\gamma)^{198}\text{Au}$  reaction, considered as "standard" between 0.2 and 3.5 MeV. Often the cross sections are safely used as standards far beyond these upper limits. By changing the sample under study and the reference gold sample frequently, one measures the incident flux quasi-simultaneously. This technique is well established by the experiments with the Karlsruhe  $4\pi$  100%  $\text{BaF}_2$  crystal ball. In the high energy domain

it is possible to determine the flux by the  $^{238}\text{U}(n,f)$  and  $^{209}\text{Bi}(n,f)$  reactions, standards from 1-200 MeV and 35-130 MeV respectively [3]. Such an on-line flux detector can be implemented as a thin foil of Mylar (about 1  $\mu\text{m}$  thick) with a deposit of a few tens of  $\mu\text{g}/\text{cm}^2$  of  $^6\text{Li}$ ,  $^{10}\text{B}$ ,  $^{235}\text{U}$ ,  $^{238}\text{U}$ ,  $^{209}\text{Bi}$ . The emitted alpha particles and fission fragments can be detected by 100  $\mu\text{m}$  thick, small and thin-windowed silicon detectors. In order to use these reactions it is possible to use an on-line flux shape detector in the way as indicated in figure 1.

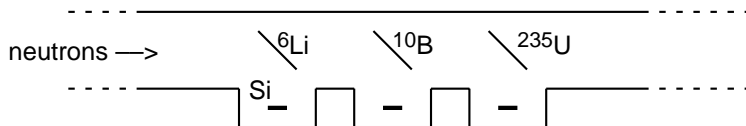


Figure 1: Schematic view of the on-line flux detector, used to measure the shape of the flux spectrum simultaneously with the capture measurement. The Mylar foils with the deposits of  $^6\text{Li}$ ,  $^{10}\text{B}$  and  $^{235}\text{U}$  are placed in the vacuum neutron flight tube. The Si detectors are also placed in the vacuum.

Additional back-to-back Si detectors would allow coincidence measurements between both reaction products, providing thus an additional constrain to the neutron energy measurement. The information of the sum signal from coincident pulses would serve to determine and reduce the possible backgrounds. An additional peak could be observed at 4.78 MeV from time non-correlated pulses induced by neutrons whose energy has been reduced to the thermal region by moderation in the walls. Similarly, a neutron energy measured from the  $\alpha$ - and t- energies in disagreement with the time information from the TOF, would arise from the energetic neutrons scattered in the walls or the beam pipe. This redundant neutron energy information from the Si detectors and the TOF would be valuable in determining both the background level and the background spectrum. These detectors should be placed as close as possible to the sample in order to measure the incident flux shape without systematic uncertainties.

### 3 The spatial profile of the neutron beam

The neutron beam profile, homogeneity, energy dependence and halo play a predominant role in the quality of the measurements and the operation of any of the planned detectors, in particular the high resolution calorimeters and HPGe detectors. Moreover, the limited size of the samples, related to their radioactivity and/or availability, implies a small size beam with well known dimensions and intensity shapes. The experimental determination of these quantities requires very low mass neutron detectors with highly segmented structure, in order to provide satisfactory spatial and time resolution. For such measurements we intend to use fission detectors with high spatial resolution and  $^6\text{Li}/^{10}\text{B}$  detectors equipped with high spatial resolution ionisation chambers.

Such fission detectors should satisfy three conditions: i) low mass for avoiding backgrounds from scattered neutrons, ii) fast response and timing and iii) sensitivity only to strongly ionising particles. The Parallel Plate Avalanche Counters (PPAC) detectors [4], already successfully used in heavy ion experiments, fulfil all of these requirements. On each side of the fissionable "standard" material, also placed perpendicularly in the beam flux, are positioned two 20x20  $\text{cm}^2$  Parallel Plate Avalanche Counters (PPAC) able to detect and measure the position of the two fission fragments emitted in coincidence by

the fissionable nuclei with practically 100% efficiency. The distance between the PPACs and the 300  $\mu\text{g}/\text{cm}^2$  target will be of 5mm.

As PPACs operate at very low gas pressure (7mbar), the sample and the PPACs will be placed inside the vacuum tube. It is possible to achieve a very good spatial resolution with these avalanche parallel plate detectors. The detectors will be made with strips every two millimeters by deposited gold on 0.9  $\mu\text{m}$  Mylar foils placed on each side of an anode made of a similar Mylar foil with gold on both sides. Therefore they are transparent to neutrons and  $\gamma$ -rays and are not sensitive to radiation damage. PPACs are the thinnest available timing and position sensitive detectors. The PPACs anodes are connected to current preamplifiers delivering 10ns signals total width to be used for the time-of-flight measurement. The strips of the cathodes are connected to delay lines, each cell of which inducing a 5ns delay, allowing a position determination from the delayed signals collected at each end of the delay lines. All signals enter 200 MHz Fast ADCs. Signal amplitude measurement and detection of the two fission fragments in coincidence will do the discrimination between fission and alpha particle emission.

The solid angle covered by these PPACs is almost  $4\pi$ . However, when the fission fragments are emitted tangentially, their self-absorption in the target, their energy loss in the backing for one of them and their energy loss in the entrance windows of the PPACs limit their detection efficiency. The table 1 shows the importance of these limitations with the target thickness. From simulations we concluded that 300 $\mu\text{g}/\text{cm}^2$  thick targets constitute a good compromise. The neutron energy is given by the time of flight (200m) between the target and the PPAC anodes. With a PPAC, a 250ps FWHM resolution is obtained after correction of delay dependence with position (which can reach 1ns). One might have also to take into account the time taken by the fragment to go from the target to the PPAC anode. In worse cases, this time is of the order of 2ns. Consequently, the time resolution is completely limited by the 6ns proton beam start signal, that is after 200m time of flight,  $10^{-4}$  for low energy neutrons and  $10^{-3}$  for very energetic neutrons.

Table 1: Variation of the setting efficiency with target thickness

Target Thickness $\mu\text{g}/\text{cm}^2$	Proportion of Fission Fragments detected with more than 10MeV residual energy inside PPAC		Angular limitation Angle between fragment and target surface	
	Facing the target	Through backing	Facing the target	Through backing
100	93.3%	83.2%	4.6°	9.1°
300	91.8%	81.7%	6.7°	10.7°
500	90.3%	80.1%	7.9°	12.4°
800	87.3%	77.0%	10.6°	14.8°
500	82.4%	69.6%	14.8°	17.8°
1000	78.84%	65.8%	16.3°	21.7°
1500	69.44%	56.5%	21.7°	26.2°
2000	61.04%	49.3%	28.6°	34.0°

Micromegas detectors will be used for the  $^{10}\text{B}(\text{n},\alpha)^7\text{Li}$  and  $^6\text{Li}(\text{n},\alpha)^3\text{H}$  reactions, where the reaction products will ionise the  $\text{CF}_4$  gas and the amplification take place in the micromesh grid. Since the neutron energy is not determined from the energy of the

alpha and tritium, this method is quite sensitive also for neutron energies below several hundred keV. The reactions,  ${}^6\text{Li}(n,n'\alpha)\text{p}$  and  ${}^6\text{Li}(n,p)$ , becoming dominant at energies above 2.5 MeV provide a continuum of deposited energy even for monoenergetic incident neutrons, but without affecting the measurement of the neutron energy by TOF. On the contrary these reactions extend the sensitivity of the detector to even higher energies. The low mass, the excellent timing and the spatial resolution of Micromegas guided our choice, which will be tested the first week of March at the monoenergetic neutron beams at Bordeaux.

#### 4 Filter changer for background measurements

Flux measurements are based on reaction with smooth cross sections. It is therefore not possible to determine the background from the shape of the cross section as it is the case for the capture yield of resolved resonances. Neutron flux detectors can be made rather insensitive to gamma-ray backgrounds. Neutron backgrounds consists of ambient neutrons from the shielding and surrounding materials and of neutrons in the beam that do not have a clear relation between their kinetic energy and their time-of-flight. The presence of such neutrons may originate from long tails in the resolution function.

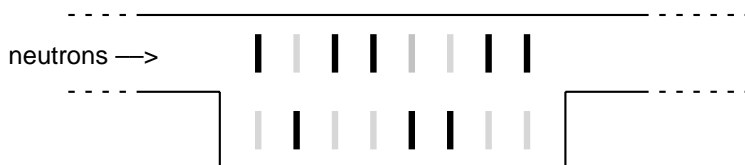


Figure 2: Schematic view of the filter changer used to measure neutron backgrounds. The filters can remotely be put in and out of the neutron beam. The whole configuration is placed within the vacuum.

Table 2: Isotopes from natural elements that can be used as black filters. Also  ${}^{73}\text{Ge}$  (102.6 eV),  ${}^{103}\text{Rh}$  (1.3 eV),  ${}^{113}\text{Cd}$  (0.18 eV),  ${}^{109}\text{Ag}$  (5.1 eV),  ${}^{197}\text{Au}$  (4.9 eV),  ${}^{195}\text{Pt}$  (11.9 eV) and  ${}^{238}\text{U}$  (several) can be used as black resonance filters.

natural element	isotope	resonance energy (eV)	nat. elem. thickness (g/cm <sup>2</sup> )
W	182	4.1	1.16
W	186	18.8	1.16
Co	59	132	0.18
Mo	95	44.7	1.2
Mn	55	336	0.7
Mn	55	1098	0.7
Bi	209	803	7.3
Bi	209	2310	7.3
Na	23	2850	0.9
S	32	30380	10
S	32	55680	16.4
Si	28	112180	10

The only way to verify this and to have access to this type of background is to put filters in the neutron beam containing isotopes with so-called "black" resonances, removing selectively neutrons from the beam. The large resonance at specific energies make

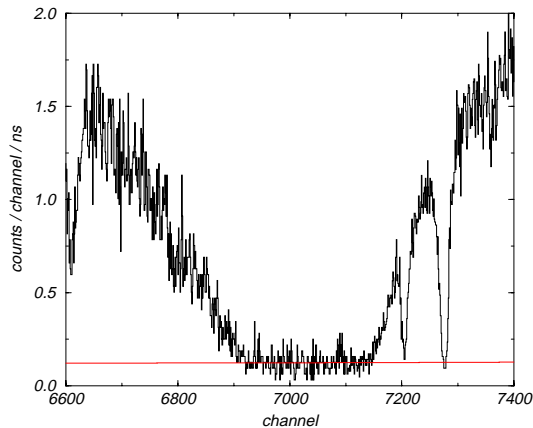


Figure 3: Typical TOF spectrum of the  $^{10}\text{B}$  chamber neutron flux detector with a black resonance in the neutron beam to measure the background, in this case the 132 eV resonance of  $^{59}\text{Co}$ . Data measured at JRC/IRMM-Geel.

that all neutrons undergo an interaction at the resonance energy and have a transmission coefficient close to zero. Therefore a "filter changer" should be put into the beam, as far as possible upstream the on-line flux detector in order to avoid the detection of neutrons scattered from these filters. For a correct study of this type of background, several combinations of filters should be used. For this reason, the "filter changer" should have several positions, as illustrated in figure 2. The diameter of these filters should be larger than the projection of the flux detector on the filters. A typical example of such a black resonance measured with a flux detector at JRC/IRMM-Geel is shown in figure 3. Also for capture measurements in the unresolved resonance region black filters in the beam will be used to determine the background. Elements with isotopes having such resonances up to 100 keV are given in the previous table.

## 5 The principle of neutron capture measurements with $\text{C}_6\text{D}_6$ detectors

The neutron capture experiments in this initial phase will be performed using  $\text{C}_6\text{D}_6$  gamma-ray detectors together with a pulse height weighting technique. Pulse height weighting is a method of making the detection efficiency independent of the gamma-ray cascade of the  $(n,\gamma)$  reaction. These detectors have a low gamma-ray efficiency of about 2% over the range of interest between 0.1-10 MeV, but are not sensitive to scattered neutrons as compared to other gamma-ray detectors. However, in contrast to a  $4\pi$  total absorption calorimeter, it is not possible with  $\text{C}_6\text{D}_6$  detectors to distinguish whether the detected gamma rays originate from the  $(n,\gamma)$  reaction, the radioactive background or from competing reaction channels like fission or inelastic scattering. The quantity determined in a neutron capture experiment is the capture yield, i.e. the fraction of neutrons incident on a sample (with thickness  $n$  atoms per barn) and undergoing the  $(n,\gamma)$  interaction. The capture yield  $Y(E)$ , with  $0 < Y(E) < 1$ , for the first interaction can be written as

$$Y(E) = (1 - e^{-n\sigma_T(E)}) \cdot \frac{\sigma_\gamma(E)}{\sigma_T(E)} \approx \begin{cases} n \cdot \sigma_\gamma & \text{if } n \cdot \sigma_T \ll 1 \\ \sigma_\gamma / \sigma_T < 1 & \text{if } n \cdot \sigma_T \gg 1 \end{cases} \quad (1)$$

The two limiting cases are approximations for thin respectively thick samples. Additional terms must be added to this yield coming from neutrons that are scattered one

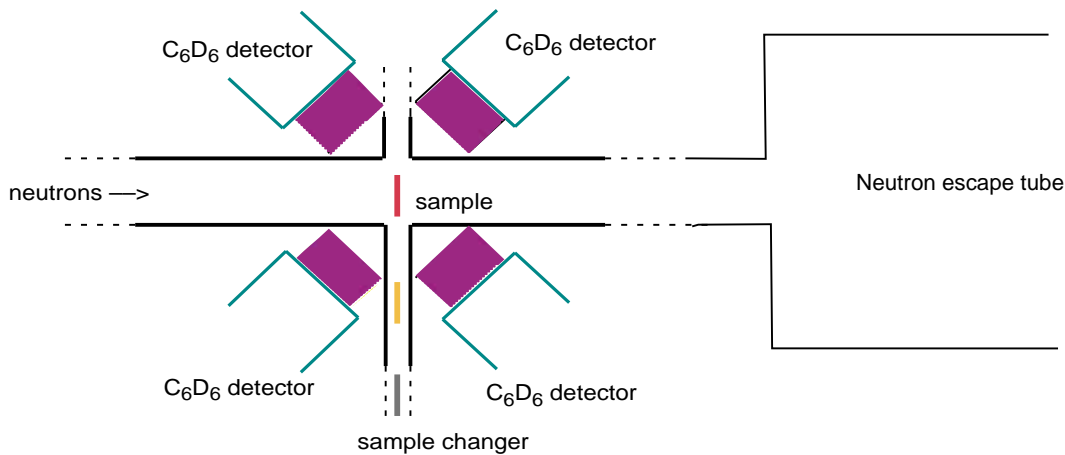


Figure 4: The set-up of the  $C_6D_6$  detectors together with the in-vacuum sample changer. The 4 detectors are all placed in air with an angle of  $135^\circ$  with respect to the neutron direction.

or more times in the sample and surroundings and subsequently captured. This multiple scattering effect has to be taken into account in the  $R$ -matrix analysis code. Since the efficiency of the capture detector and solid angle of the detector do not exceed few percents, the measured time-of-flight spectra need to be normalised to a well known isotope in order to extract the normalisation constant, representing the solid angle and the detector efficiency. The standard technique is to measure this normalisation using a "saturated" resonance. This refers to a resonance where the thick sample approximation is valid in the peak of the resonance and where the capture yield is no more proportional to the capture cross section but to the ratio of the capture and the total cross section. The measured resonance shape has then a flat top and from this characteristic shape the normalisation constant can be extracted. Often an isotope does not have such a large resonance or is not available in a thick sample. In that case the normalisation is determined by measuring the first saturated resonance of e.g. gold or silver at resonance energies of 4.9 eV ( $^{197}\text{Au}$ ) and 5.1 eV ( $^{109}\text{Ag}$ ) respectively. Since only the saturated resonance needs to be measured, the normalisation measurement with gold or silver lasts in general much shorter than the actual measurement. We intent to use a set of 4 BC537  $C_6D_6$  gamma-ray detectors, each coupled to a XP4512B photomultiplier. They will be placed under an angle of 135 degrees with respect to the neutron flight direction in order to reduce angular distribution corrections. The detectors are fixed by a simple strap fixation of the photomultiplier housing to a low mass aluminum frame. The samples to be measured, disc shaped with a diameter ranging from typically 3 to maximum 8 cm, are placed in a carbon fiber sample changer which is connected to the vacuum neutron guide, also made of carbon fibre in the area of the detector station. Figure 4 shows a sketch of the planned detector and sample set-up.

## 6 Determination of weighting functions

The working principle [5] of the  $C_6D_6$  detectors for  $(n,\gamma)$  cross-section measurements, is the *a posteriori* manipulation of their  $\gamma$  response distribution  $R_{ij}$  through the introduction of a set of weighting factors  $W_i$  such that the detection efficiency becomes

proportional to the  $\gamma$ -ray energy  $E_{\gamma_j}$

$$\sum_i W_i R_{ij} = k E_{\gamma_j} \quad (2)$$

In this way the detection efficiency of the capture cascade becomes proportional to the energy of the cascade, and thus independent of the actual path, if the probability of simultaneous detection of more than one cascade  $\gamma$ -ray is negligible.

Obviously the accuracy of the result depends on the accuracy with which the response distributions could be determined in the range of energies of interest (up to 10 MeV). Initially these were calculated by Monte Carlo (MC) simulation, but it was subsequently found that there existed considerable discrepancies between the results of this technique and those obtained from transmission measurements and that the reason for the discrepancy was to be found in the inadequacy of the MC result [6]. An experimental weighting function was determined from (p, $\gamma$ ) measurements and their use for the capture measurements proposed [7]. At the same time it was demonstrated the sensitivity of the response distributions to the experimental set-up, therefore limiting the use of this weighting function.

Recently [8] we have used the GEANT3 MC package [9] to calculate the response distributions for the (p, $\gamma$ ) set-up of Ref. [7] and could obtain a good reproduction of the shape of the measured distributions. We were also able to determine that it was actually the tantalum backing of the targets the one introducing the strongest perturbation on the response. These all lead to the conclusion that the only practical way to take into account the different measuring conditions (samples) in different experiments will be to use specific Monte Carlo derived weighting functions. The accuracy of the weighting functions obtained by the Monte Carlo method has to be checked in real experimental conditions.

Therefore we propose to measure resonances with simple decay patterns (16.2 keV and 30.4 keV in  $^{207}\text{Pb}$ ) which allow a direct check of the response distributions. We also propose to perform a systematic study of the cross-section obtained for the well known 1.15 keV resonance in  $^{56}\text{Fe}$  (which appears to be particularly sensitive to the correct weighting function) varying the sample thickness and composition (0.5 and 1.0 mm Fe, 0.5 mm  $\text{Fe}_2\text{O}_3$  and 0.5 mm/0.1 mm Fe/Au sandwich). From the calculated counting rates in the resonances we have estimated that a total of 25 days of beam time would be necessary to complete these measurements.

## 7 On-line flux determination in (n, $\gamma$ ) measurements

To reconstruct the capture yield from the measured time-of-flight spectra it is necessary to determine the incident neutron fluence, i.e. the flux integrated over the measurement time. In fact the knowledge of the shape of the neutron flux as a function of the time-of-flight is required, but not the absolute value. The scaling factor for the absolute flux is conveniently taken in the normalisation, which is fitted, from a saturated resonance in the capture spectrum. Since at the existing neutron TOF installations instabilities in the energy dependence of the flux are routinely observed, capture experiments have been greatly improved by measuring the shape of the flux simultaneously with the capture measurement. However, we do not expect at the CERN spallation source such variations experienced at Electron Linacs.

## 8 Resolution function and energy calibration

The neutron kinetic energy is directly related to the flight time of the neutron and the flight length. The distribution of the detected time-of-flight or equivalently the effective flight distance for a neutron of a given energy is called the resolution function. This resolution function has several components related to the different processes contributing to the total resolution.

The time distribution of the initial proton pulse is the first component to be taken into account. Then the process of slowing down in the lead target and subsequently the moderation of the neutrons in the water adds to the resolution. Also the detector may contribute to the TOF width to be included in the resolution.

Some of the resolution components may have highly non-Gaussian distributions. In fact the water moderation is often associated with a chi-square distribution with a small number of degrees of freedom. Also long exponential tails have been observed at several other TOF installations. Since the resolution expressed in equivalent flight distance has a maximum depending from the neutron energy, the relation between the neutron kinetic energy and the time-of-flight is less straightforward and requires the exact knowledge of the resolution.

The total resolution is formed by the convolution of the individual components. From the known physical processes and from Monte Carlo simulations a modelling of the resolution function is established. The parameterisation of this model has to be fitted from measured data. A good knowledge of the resolution function is important for fitting the resolved resonances. For smooth cross sections in the unresolved resonance range, resolution clearly is less important.

The natural width of a resonance is broadened by two phenomena. The first one is the Doppler broadening due to the thermal motion of the target nuclei. For most single elements the Doppler broadening is well described by the so-called free gas model with an effective temperature (with respect to this it should be noted that the temperature of the target should be monitored and preferably kept constant). This Doppler width increases with the square root of the energy. If the target nuclei are embedded in more complicated chemical compounds, more sophisticated Doppler broadening models are necessary. The second cause of broadening is due to resolution that becomes the predominant effect at higher energies, whereas at lower energies the Doppler broadening is the largest effect.

Isotopes that are well suited to determine the resolution over a large energy range are  $^{238}\text{U}$  and  $^{56}\text{Fe}$ . In the resolved energy range where the cross section is described in terms of resonance parameters, the isotope  $^{238}\text{U}$  is well known. Also, several narrow resonances of  $^{238}\text{U}$  are commonly used as neutron energy "standard". At low energies (below 1 or 2 keV) these resonances can be used to determine the resolution. It is preferable to use depleted uranium to avoid the resonance structures of  $^{235}\text{U}$ .

The large level spacing of  $^{56}\text{Fe}$  makes it possible to measure resolved resonances up to at least 200 keV which can be used to determine the resolution. The resolution function is in general not a Gaussian. At higher energies the Doppler broadening becomes much smaller than the resolution broadening which is therefore easier to determine. The resolution parameters should be fitted from the measured capture yield by an  $R$ -matrix analysis including an adequate modelling of the resolution function.

## 9 The sample changer for background determination in $(n,\gamma)$ experiments

Neutron time-of-flight measurements of  $(n,\gamma)$  cross sections have to face  $\gamma$ -backgrounds from various sources. For achieving high precision results, the corresponding corrections

require as much experimental information on these background components as possible.

A successful way of collecting this information is the use of a "sample changer". It allows to study, quasi-simultaneous with the sample under investigation, both background components, the general environmental background and the background due to scattered neutrons. The first component can be determined by means of an empty position or by using an empty sample container. The second component can be simulated by a carbon or a  $^{208}\text{Pb}$  sample, which have negligible  $(n,\gamma)$  cross sections. Moreover, a reference sample of  $^{197}\text{Au}$  is installed for measuring the neutron flux by the same reaction type and with the same detector set-up. We will build a "sample changer" similar to the design in use at the Karlsruhe  $4\pi$   $\text{BaF}_2$  detector, operating with stepping motors by remote computer control. However, contrary to the existing version, our design considers that at the n\_TOF facility the samples are inside the evacuated flight tube. Therefore, a cross in the neutron flight tube is to be used for moving the sample ladder vertically through the beam. All materials have to be minimised and have to be chosen for the smallest possible neutron capture cross sections. In order to match the various beam diameters that are foreseen for capture experiments, two geometries are envisaged serving sample diameters up to 80 mm and up to 20 mm. The second solution is to be designed in such a way that it can be used in a future  $4\pi$  calorimeter as well.

The construction will be based on Monte Carlo simulations minimising possible backgrounds from the interaction of scattered neutrons with the various parts of the "sample changer". These results have to be verified by test experiments using a set of different samples.

## 10 Testing a $\text{BaF}_2$ array at the CERN n\_TOF facility

### 10.1 Techniques for $(n,\gamma)$ studies - possibilities and limitations

The experimental methods for measuring  $(n,\gamma)$  cross sections fall into two groups, time-of-flight (TOF) techniques based on the detection of the prompt capture  $\gamma$ -rays and activation methods.

Compared to the activation methods, TOF measurements have the advantage that large neutron energy intervals can be studied and that there are very few limitations concerning the accessible samples. In TOF experiments, capture events are identified by the prompt  $\gamma$ -ray cascade in the product nucleus. However, only for very light isotopes, these cascades are sufficiently well defined that single  $\gamma$ -transitions can be used as a good signature for capture events [10, 11].

In the vast majority of reactions the cascade multiplicity exhibits a random behavior due to the large number of decay channels for the compound state. Accordingly, corrections for the unknown cascade multiplicity are important if detectors with modest  $\gamma$ -ray efficiency, e.g. Moxon-Rae detectors [12] or total energy detectors [13], are applied.

Total energy detectors based on  $\text{C}_6\text{D}_6$  liquid scintillation counters in combination with the pulse height weighting technique are commonly used at electron linacs, for example in the measurements of Refs. [14, 15]. Built from materials with very small neutron capture cross sections and due to their relatively small scintillator volume of about 1 l, these detectors stand out for their very low sensitivity to scattered neutrons. Accordingly, they are well suited for measurements on nuclei with very large scattering to capture ratios, i.e. in the mass region below Fe or at magic neutron numbers. On the other hand, these detectors suffer from inherent problems which result from their poor energy resolution and their small efficiency. Accordingly, background discrimination and systematic effects due to peculiarities of the prompt  $\gamma$ -ray cascade are difficult to handle, leading to

typical cross section uncertainties of 3 to 5%.

The best signature for the identification of neutron capture events is the total energy of the capture  $\gamma$ -ray cascade which corresponds to the binding energy of the captured neutron. Hence, accurate measurements of  $(n,\gamma)$  cross sections require a detector that operates as a calorimeter with good energy resolution. In the  $\gamma$ -spectrum of such a detector, all capture events would fall in a line at the neutron binding energy (typically between 5 and 10 MeV), well separated from the  $\gamma$ -ray backgrounds that are inevitable in neutron experiments. Additional information on capture events can be obtained via the cascade multiplicities.

These arguments point to a  $4\pi$  detector of high efficiency and granularity, made of a scintillator with reasonably good time and energy resolution. In addition, the detector should be insensitive to scattered neutrons, since the scattering cross sections are on average about 10 times larger than the capture cross sections. These aspects have been combined in the design of the Karlsruhe  $4\pi$  BaF<sub>2</sub> array consisting of 42 independent detector modules. The  $\gamma$ -ray efficiency of this detector is better than 90% in the entire energy range below 10 MeV. Consequently, capture events can be detected with almost 100% probability [16, 17]. Together with the good resolution in  $\gamma$ -ray energy as well as in TOF this feature is essential for the 1% accuracy that is achieved in cross section measurements with this detector.

A BaF<sub>2</sub> array is also well suited for a variety of other experiments. For example, the capture cross section of a fissile sample can be determined because capture and fission events can be separated by their different  $\gamma$ -ray patterns. It may also be useful for measuring inelastic cross sections or can serve as a  $\gamma$ -trigger in more complex experiments.

## 10.2 A $4\pi$ detector for the n\_TOF facility

The option to build a  $4\pi$  detector for the n\_TOF facility was investigated on the basis of the Karlsruhe design. Detailed GEANT simulations of the full setup were performed using the original capture cascades, which were obtained either from the ENDF/B library that is part of the GEANT software or from detailed theoretical calculations. The results for metallic gold samples could be directly compared to experimental spectra since such samples are routinely used for neutron flux measurement in the Karlsruhe setup. In simulating the background from scattered neutrons, capture events in the various barium isotopes as well as in fluorine and reflector materials were considered.

Figure 5 shows the comparison between the experimentally measured sum-energy spectra of neutron captures in the gold sample [18] and the corresponding simulation. The spectra show two components: capture cascades which are completely detected and appear as a line at the binding energy of the captured neutron, and events where part of the energy of the cascade  $\gamma$ -rays escapes detection resulting in a tail towards lower energies. Both components are reproduced very well by the simulation.

In a further step, the performance of this detector was simulated under the conditions of the n\_TOF facility. In contrast to the setup at Karlsruhe, the much larger neutron flight path does no longer allow an efficient TOF discrimination of the crucial background from sample-scattered neutrons. Assuming the Karlsruhe  $4\pi$  BaF<sub>2</sub> detector at the 200 m station of the n\_TOF facility, capture events in a <sup>197</sup>Au sample are compared in figure 6 with the background from neutrons scattered in that sample. For time-of-flight cuts corresponding to energy intervals from 0.1 to 1 keV, 1 to 10 keV, and 10 to 100 keV this scattering background (hatched area) can certainly be handled since it exhibits a significantly different shape than the spectrum of capture events in the gold sample, and

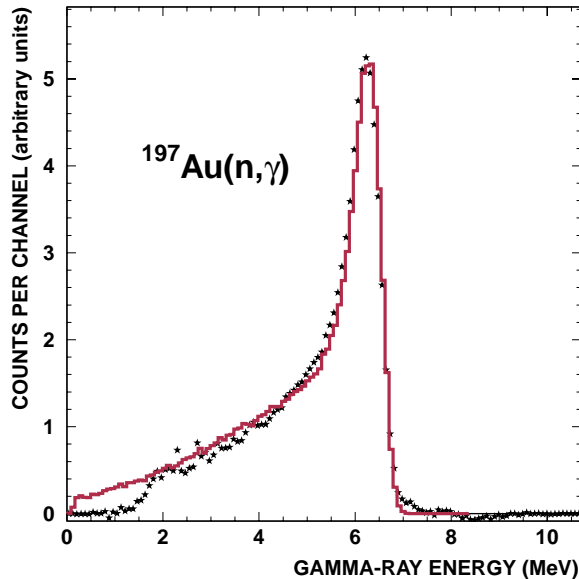


Figure 5: GEANT simulation of the  $\gamma$ -response of the Karlsruhe  $4\pi$  BaF<sub>2</sub> detector to capture events in  $^{197}\text{Au}$  (stars) compared with the measured spectrum (histogram). The excellent agreement confirms that the complex experimental situation can be reliably simulated.

since this shape can be accurately determined by means of a carbon sample.

The signal-to-background ratio shown in Fig. 2 can be further improved by an order of magnitude with a neutron absorbing layer of  $^6\text{LiH}$  surrounding the sample.

### 10.3 Test measurements with a $1\pi$ BaF<sub>2</sub> array

In order to verify the GEANT simulations at the n\_TOF facility we propose test measurements with an array consisting of 10 spare modules of the Karlsruhe  $4\pi\text{BaF}_2$  detector. The corresponding simulations in figure 7 show that the performance of a complete  $4\pi$  detector can well be studied in this way. Two geometries are to be investigated with the array sidewise and perpendicular to the neutron beam. For the second geometry, a module with a cylindrical center hole of 50 mm diameter for the neutron beam pipe is available.

These tests are planned with gold samples for which the simulations are based on well-established experimental information for the capture cascades. The additional use of carbon samples, which act as pure scattering samples with a negligible capture component, allows to measure the scattering background experimentally. A beam time of 10 days is estimated for these test measurements.

## 11 Beam Beam time request

We intend to perform the above test measurements starting from early summer 2000. These measurements will allow to determine the characteristics and backgrounds of the n\_TOF facility indispensable for any further experimentation. Moreover this initial phase will provide the necessary experience to the collaboration concerning the operation of the different detectors in this new facility.

We ask for six weeks of beam time under the normal operation of one bunch per supercycle. Our programme will clearly benefit from the possibility of more than one

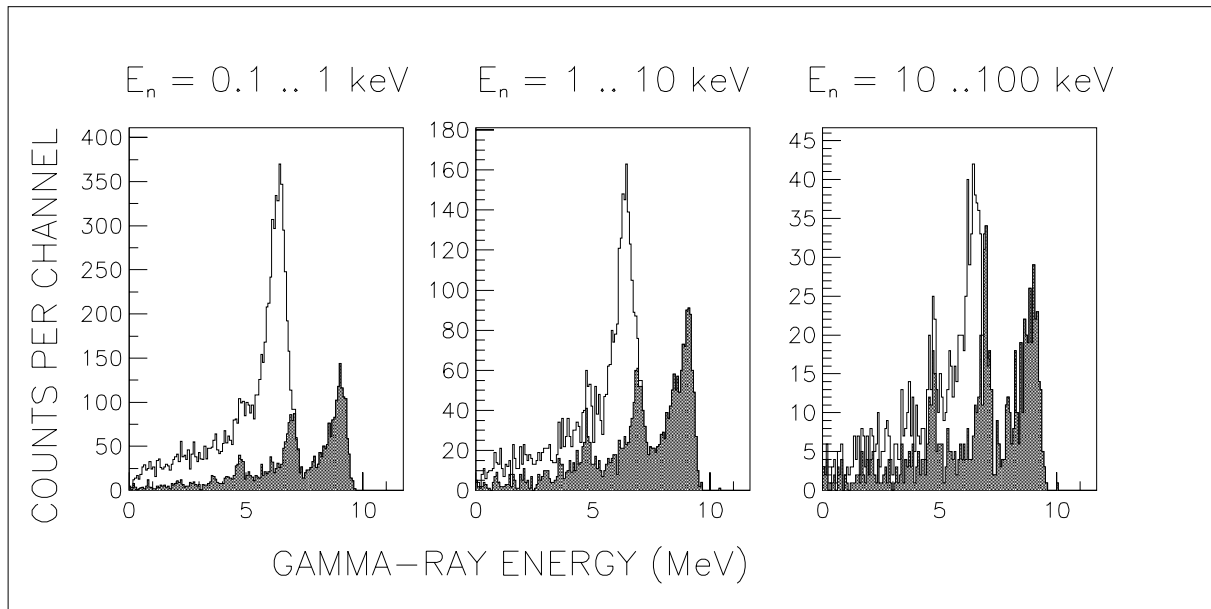


Figure 6: GEANT simulation of the performance of the Karlsruhe  $4\pi$  BaF<sub>2</sub> detector at the 200 m flight path of the n\_TOF facility. The  $\gamma$ -response to capture events in <sup>197</sup>Au (histogram) can be discriminated from background due to neutrons scattered in the sample (hatched area). With a layer of <sup>6</sup>LiH around the sample, scattered neutrons can be efficiently suppressed resulting in a ten times better signal-to-background ratio

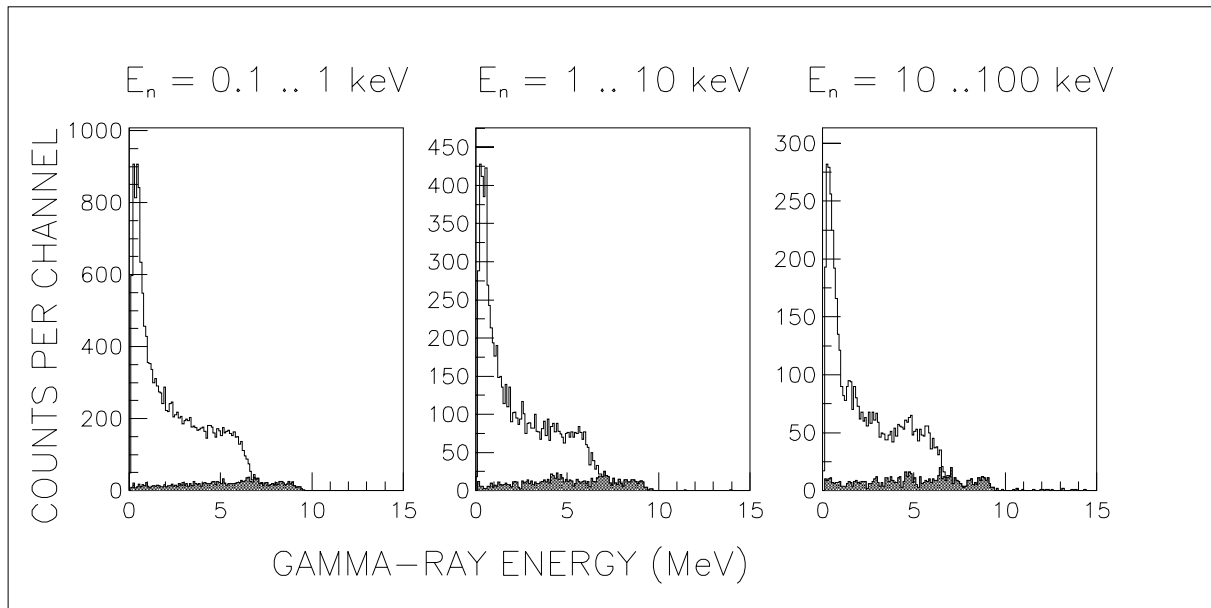


Figure 7: GEANT simulation of capture events in a gold sample measured with a subset of the Karlsruhe  $4\pi$  BaF<sub>2</sub> detector. This array consists of 10 modules and covers 1/4 of the full solid angle. Time-of-flight cuts are as in Fig. 6

bunch per supercycle.

## References

- [1] The n\_TOF Collaboration, “Proposal for a neutron time-of-flight facility”, CERN/SPSC 99-08, SPSC/P310, March 1999.
- [2] *Nuclear Data Standards for Nuclear Measurements* NEANDC-311 “U”, INDC(SEC)-101, 1992
- [3] H. Schumacher, private communication
- [4] C. Stephan in “Experimental Techniques in Nuclear Physics”, eds D.N.Poenaru and W.Grenier, Walter de Gruyter, 1997.
- [5] R. L. Macklin et al., *Phys. Rev.* **159** (1967) 1007
- [6] F. Corvi et al., *Nucl. Instr. and Meth.* **A265** (1988) 475
- [7] F. Corvi et al., *Nucl. Sci. and Eng.* **107** (1991) 272
- [8] J. L. Tain et al., *IFIC preprint 2000-11*  
<http://fachp1.ciemat.es/ntofmc/documents/documents.html>
- [9] GEANT: Detector description and simulation tool, CERN Program Library W5013, Geneve, 1994.
- [10] Y. Nagai *et al.*, *Ap. J.* **381**, 444 (1991).
- [11] M. Igashira *et al.*, *Ap. J.* **441**, L89 (1995).
- [12] S. Jaag and F. Käppeler, *Phys. Rev. C* **53**, 2474 (1996).
- [13] R. Macklin and J. Gibbons, *Phys. Rev.* **159**, 1007 (1967), includes H. Maier-Leibnitz, priv. comm. and Rau63.
- [14] P. Koehler *et al.*, *Phys. Rev. C* **54**, 1463 (1996).
- [15] H. Beer, F. Corvi, and P. Mutti, *Ap. J.* **474**, 843 (1997).
- [16] K. Wisshak *et al.*, *Nucl. Instr. Meth. A* **292**, 595 (1990).
- [17] K. Wisshak *et al.*, *Phys. Rev. C* **52**, 2762 (1995).
- [18] K. Wisshak, F. Voss, F. Käppeler, and G. Reffo, *Phys. Rev. C* **45**, 2470 (1992).